J. Fluid Mech. (2004), *vol.* 513, *pp.* 287–307.
DOI: 10.1017/S0022112004009954 Printed in the United Kingdom

Flame holes and flame disks on the surface of a diffusion flame

By ZHANBIN LU† AND SANDIP GHOSAL

Department of Mechanical Engineering, Northwestern University,
2145 Sheridan Road, Evanston, IL 60208, USA
s-ghosal@northwestern.edu

(Received 8 July 2003 and in revised form 9 April 2004)

Flame holes and flame disks in a laminar axisymmetric counterflow configuration are numerically investigated for unity Lewis number, with the strain rate as the control parameter. The temporal evolution of the topological structure of flame holes and flame disks is described in detail for different representative strain rates. It is found that corresponding to each given strain rate, there exists a critical hole (disk) radius r_c that separates the shrinking and expanding hole (disk) regimes. The value of r_c decreases monotonically with the increase (decrease) of strain rate and reaches a finite minimum at the extinction (ignition) limit of the strain rate, which indicates that one cannot ignite a mixing layer by an infinitesimal energy source, nor can one quench a diffusion flame by making an infinitesimal extinction hole on it. An examination of the phase diagrams of flame holes (disks) justifies the existence of a unique edge-flame velocity v_f as a smooth continuous function of the hole (disk) radius r_f in the entire range $0 < r_f < \infty$, with the strain rate (or equivalently, Damköhler number) as a parameter. For the flame hole case, it is found that in the final stage of collapse of a hole, the edge-flame velocity is essentially proportional to the inverse of the hole radius, except when the strain rate is very close to the extinction limit. Flame interactions induced by overlapping of pre-heat zones are mainly responsible for the acceleration of the edge-flame velocity when the hole radius approaches zero, and it is further enhanced by the focusing effects of hole curvature in the plane of the stoichiometric surface. For the flame disk, the increasing heat loss rate plays a major role on the acceleration of the shrinking speed when the disk radius approaches zero.

1. Introduction

Local extinction and re-ignition are ubiquitous phenomena in turbulent diffusion flames. One important approach to modelling turbulent diffusion flames is the flamelet model, in which turbulent diffusion flames are described as consisting of an ensemble of stretched laminar flame sheets, or flamelets. The concept of a flamelet was first proposed by Williams (1975) and later developed by Peters (1983) to study the local quenching and re-ignition behaviour in turbulent diffusion flames. According to Peters (1983), local extinction and re-ignition of a turbulent diffusion flame are controlled by the local Damköhler number, which may be constructed based on the dissipation rate

† Present address: Department of Aerospace engineering, University of Illinois at Urbana-Champaign, 104 S. Wright Street, Urbana, IL 61801, USA.

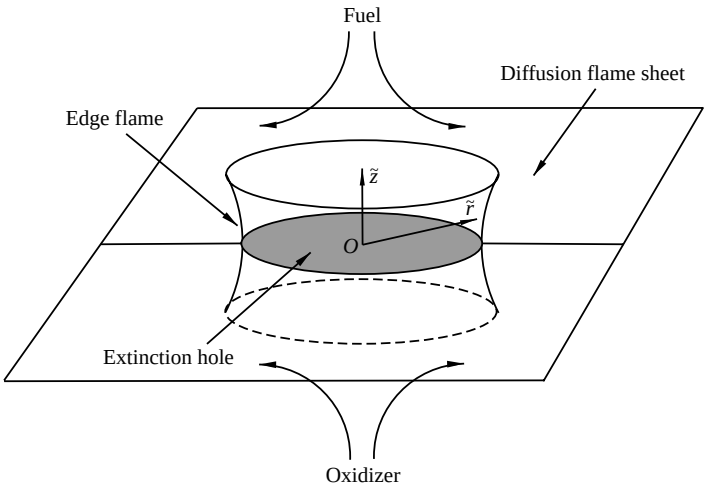

FIGURE 1. Schematic diagram of the structure of an extinction hole on an axisymmetric counterflow diffusion-flame sheet.

of a scalar – the mixture fraction. The scalar dissipation rate is directly proportional to the strain rate. If the scalar dissipation rate is locally above a critical value, extinction occurs in the neighbourhood of that point, appearing as an 'extinction hole', or synonymously, a 'flame hole' on the flame sheet. Once the scalar dissipation rate returns to below the critical value in the vicinity of the extinction hole, the surrounding flame elements may propagate inward to re-ignite the extinguished area. Since in a turbulent flow field the scalar dissipation rate is a stochastic variable, it leads to a time-varying random distribution of extinction holes on turbulent diffusion flame sheets. Such local quenching and re-ignition phenomena have been observed (see e.g. Schefer *et al.* 1994) in the laboratory using flame visualization techniques. In recent years, numerous numerical works have been devoted to the study of such local extinction and re-ignition events in turbulent diffusion flames using the flamelet formulation (Mauss, Keller & Peters 1990; Pitsch & Fedotov 2001; Pitsch, Cha & Fedotov 2003) or conditional moment closure (CMC) modelling (Cha, Kosaly & Pitsch 2001; Cha & Pitsch 2002; Kim, Huh & Bilger 2003).

There is another phenomenon, 'flame disks', which is closely related to 'flame holes' in turbulent diffusion-flames. A flame disk is a small burning element that may serve as an ignition source along the stoichiometric surface to re-ignite the extinguished area. Domingo & Vervisch (1996) investigated the 'auto-ignition' process of non-premixed turbulent mixtures from an ignition kernel using two-dimensional direct numerical simulations. Their work provides a description of the cross-sectional structure of flame disks in a turbulent environment.

In the context of the laminar flamelet model, the investigation of flame holes and flame disks in a laminar flow environment may be of underlying significance for turbulent flame studies. Figure 1 shows a schematic diagram of the topological structure of a flame hole on a laminar axisymmetric counterflow diffusion-flame sheet. A characteristic structure, the edge flame, develops at the interface between the burning and extinguished regions, as shown in figure 1 in cross-section. Depending on the strain rate, the edge flame may exhibit different structural features. When the strain rate is relatively small, the edge flame is characterized by a tribrachial structure – two curved partially premixed flame branches joined with the diffusion

flame branch at a single point – hence in this context the edge flame is also called a 'tribrachial flame' or 'triple flame'. This is the case shown in figure 1. However, if the strain rate parameter is increased, the two partially premixed branches gradually 'fold' onto the diffusion flame branch, eventually degenerating into a simple blunt edge. The most important dynamical characteristic of the edge flame is that it has an ability to propagate, with a speed either positive (ignition front) or negative (extinction front or failure wave), depending on the strain rate and the curvature of the edge. Straight (zero curvature on the diffusion-flame plane) edge flames have been studied extensively in the literature. The first report of laboratory observations of a triple flame is attributed to Phillips (1965). In recent years, a number of experimental (Kioni *et al.* 1993; Lee & Chung 1997; Plessing *et al.* 1998; Shay & Ronney 1998; Ko & Chung 1999) and numerical (Ruetsch, Vervisch & Liñán 1995; Domingo & Vervisch 1996; Favier & Vervisch 1998; Echekki & Chen 1998; Im & Chen 1999) investigations, in both laminar and turbulent flow situations, have been reported. Various theoretical works (Buckmaster & Matalon 1988; Dold 1989; Hartley & Dold 1991; Buckmaster 1996, 1997; Daou & Liñán 1998; Ghosal & Vervisch 2000) have also been devoted to the study of such two-dimensional triple (or edge) flames. A recent review of edge flames was given by Buckmaster (2002).

In turbulent flows flame edges are more likely to be curved lines on the stoichiometric surface. However, it was only recently that such curved edge flames began to receive much attention. The first theoretical investigation of the effects of curvature on the edge flame is due to Nayagam, Balasubramaniam & Ronney (1999). They extended Buckmaster's one-dimensional edge-flame model (Buckmaster 1996) to an axisymmetric diffusion-flame hole of finite radius. Their analysis showed that for 'free' flame holes (without a heat sink at the axis), at small Damköhler number, the holes either grow (as an extinction wave) or shrink (as an ignition wave) depending on whether the initial hole radius is above or below a certain critical value; for large Damköhler number, the holes shrink for any initial hole radius. They also obtained a closed-form expression for the edge-flame velocity as a function of the hole radius and the Damköhler number, by introducing an approximate quasi-steady assumption. In an experimental investigation of diffusion-flame disks, Nayagam & Williams (2001) found good agreement of the measured collapse rates with the theoretical predictions. Papas & Tomboulides (2000) performed experimental and numerical investigations of diffusion flames in a counterflow configuration. They reported the existence of two types of flame structure – a disk-shaped diffusion flame and an annular-shaped flame – and observed the hysteretic transition of these two types of flame, depending on the strain rate and the overall activation energy. Santoro, Liñán & Gomez (2000) performed an experimental investigation on the propagation of edge flames in counterflow mixing layers. They observed the existence of an annular edge flame structure by creating a flame hole on the diffusion flame sheet, and found that the edge flame quickly propagated in the radial direction and eventually stabilized as a standing triple flame. The measurement results demonstrated a correlation of the edge-flame propagation speed with the strain rate (or the Damköhler number).

Buckmaster & Jackson (2000) numerically investigated the flame hole and flame disk problems using a simple thermal–diffusive model in the absence of a straining velocity field. They studied how the shrinkage or expansion of a flame hole (disk) depends on the instantaneous hole (disk) radius and the Damköhler number, and for a given hole (disk) radius, found a critical Damköhler number at which the edge is stationary. They further examined the edge travelling speeds of flame holes and disks and concluded that for shrinking holes and disks, a unique edge propagation

speed may be defined as a function of the instantaneous hole (disk) radius for given combustion parameters.

Very recently, Pantano & Pullin (2003) studied the collapse dynamics of a diffusion flame hole with unity Lewis number and in the presence of a counterflow velocity field, also by using Buckmaster's one-dimensional edge-flame model. Their analysis showed that the final stage of flame hole collapse is determined by a dominant balance between the time rate of change of temperature and diffusion, and the effects of side losses and advection turn out to be higher-order effects. As a result, to leading order, the size of the flame hole shrinks according to a 1/2-power of time remaining to collapse in this final stage. This 1/2-power law was also obtained in our investigation of the head-on collision process of two planar premixed flames in the final stage before their mutual annihilation (Lu & Ghosal 2003).

In this paper, we will conduct a detailed numerical investigation of flame holes and flame disks in a laminar axisymmetric counterflow configuration. For simplicity, we will only consider the unity Lewis number case. Our work differs from that of Buckmaster & Jackson (2000) mainly in two aspects. First, the effects of flow fields are incorporated; secondly, the temporal evolution of the topological structure of flame holes (disks) will be explored for different representative strain rates. This will help elucidate the underlying mechanism that governs the dynamical characteristics of flame holes (disks) and how the behaviour of the system changes as the strain rate (and therefore the Damköhler number) is varied over the entire range of values between the ignition and extinction limits. Then, we will concentrate on the investigation of the dynamics of the flame holes and flame disks in the entire interesting range of strain rate, in an effort to gain an insight into the effects of hole (disk) curvature and strain rate on the dynamical properties of flame holes (disks).

The paper is organized as follows. We formulate the problem in the next section. Basic governing equations are given and then non-dimensionalized by choice of appropriate dimensionless variables. In § 3 we discuss the numerical methods we use to solve the problem. The properties of a steady flame sheet are first studied in § 4, from which the interesting range of parameters is identified and four representative cases are chosen for further study. Then, the results for flame holes and flame disks are presented in § 5 and § 6, respectively. Finally, the main results of the paper are summarized in § 7.

2. Formulation

We consider a three-dimensional incompressible axisymmetric counterflow configuration, with fuel and oxidizer supplied from opposite sides, respectively. A cylindrical coordinate system $(\tilde{r}, \phi, \tilde{z})$ is adopted, with the origin O at the stagnation point and the $\tilde{z}$-axis pointing towards the fuel side, as shown in figure 1. The counterflow velocity field has the representation $(\tilde{u}_r = a\tilde{r}, \tilde{u}_z = -2a\tilde{z})$, where $(\tilde{u}_r, \tilde{u}_z)$ are the radial and axial velocity components, and a is the strain rate parameter. Global Arrhenius chemistry is assumed so that the reaction rate

$$\omega = BY_0Y_1 \exp\left\{-\frac{E}{RT}\right\} \tag{2.1}$$

where B is a constant pre-exponential factor, E is the activation energy of the reaction, R is the universal gas constant, T is the temperature of the mixture, and $Y_i (i = 0, 1)$ are the mass fractions of the fuel and oxidizer, respectively. We assume that the fuel

and oxidizer are diluted by an inert species, so that the heat released by chemical reaction is small compared with the thermal energy of the mixture. Thus, we adopt the constant-density approximation. Furthermore, the thermal diffusivity, specific heat and density of the mixture are approximated by those of the inert component, which are constants and denoted by D_T, C_p and ρ, respectively. The conservation equations for energy and species are

$$\frac{\partial T}{\partial \tilde{t}} + a\tilde{r}\frac{\partial T}{\partial \tilde{r}} - 2a\tilde{z}\frac{\partial T}{\partial \tilde{z}} = D_T\left[\frac{1}{\tilde{r}}\frac{\partial}{\partial \tilde{r}}\left(\tilde{r}\frac{\partial T}{\partial \tilde{r}}\right) + \frac{\partial^2 T}{\partial \tilde{z}^2}\right] + \frac{Q}{\rho C_p}\omega, \tag{2.2}$$

$$\frac{\partial Y_i}{\partial \tilde{t}} + a\tilde{r}\frac{\partial Y_i}{\partial \tilde{r}} - 2a\tilde{z}\frac{\partial Y_i}{\partial \tilde{z}} = D_i\left[\frac{1}{\tilde{r}}\frac{\partial}{\partial \tilde{r}}\left(\tilde{r}\frac{\partial Y_i}{\partial \tilde{r}}\right) + \frac{\partial^2 Y_i}{\partial \tilde{z}^2}\right] - \frac{\nu_i W_i}{\rho}\omega. \tag{2.3}$$

Here Q is the heat released per reaction, D_i are the mass diffusivities, ν_i are the stoichiometric coefficients, and W_i are the molecular weights.

The boundary conditions are now specified. In the radial direction, all dependent variables are axisymmetrical and tend to a homogeneous state when $\tilde{r} \to \infty$, so we have

$$\left.\frac{\partial T}{\partial \tilde{r}}\right|_{\tilde{r}=0,\infty} = \left.\frac{\partial Y_i}{\partial \tilde{r}}\right|_{\tilde{r}=0,\infty} = 0. \tag{2.4}$$

In the transverse direction, we assume that the fuel and oxidizer have the same unburned temperature T_u and unburned mass fractions Y_{0u} and Y_{1u}, respectively. In terms of symbols, the transverse boundary conditions are

$$T(\tilde{z} \to \pm\infty) = T_u, \tag{2.5}$$

$$Y_0(\tilde{z} \to +\infty) = Y_{0u}, \quad Y_0(\tilde{z} \to -\infty) = 0, \tag{2.6}$$

$$Y_1(\tilde{z} \to +\infty) = 0, \quad Y_1(\tilde{z} \to -\infty) = Y_{1u}. \tag{2.7}$$

Once a steady diffusion flame is established, the reaction sheet is located at $\tilde{z} = \tilde{z}_s$ which defines the stoichiometric plane. In the absence of reaction ($\omega = 0$), (2.3) admits the steady solutions

$$Y_0 = Y_0(\tilde{z}) = \tfrac{1}{2}Y_{0u}\left[1 + \operatorname{erf}\left(\sqrt{\frac{a}{D_0}}\,\tilde{z}\right)\right], \tag{2.8a}$$

$$Y_1 = Y_1(\tilde{z}) = \tfrac{1}{2}Y_{1u}\left[1 - \operatorname{erf}\left(\sqrt{\frac{a}{D_1}}\,\tilde{z}\right)\right]. \tag{2.8b}$$

For simplicity we further assume that the fuel and oxidizer are equi-diffusive, i.e. $D_0 = D_1 = D$. Thus, according to the stoichiometric relation $Y_0(\tilde{z}_s)/Y_1(\tilde{z}_s) = \nu_0 W_0/\nu_1 W_1$, (2.8 *a*, *b*) can be combined to solve for $\tilde{z}_s$:

$$\tilde{z}_s = \sqrt{\frac{D}{a}}\,\operatorname{erf}^{-1}\left[\frac{1-\sigma}{1+\sigma}\right], \tag{2.9}$$

where $\sigma = Y_{0u}\nu_1 W_1/Y_{1u}\nu_0 W_0$. For the purpose of the numerical simulations presented in this paper, we will assume $\sigma = 1$ so that $\tilde{z}_s = 0$. Thus, in this case the reaction sheet is coincident with the stagnation plane.

To non-dimensionalize the conservation equations (2.2) and (2.3), we choose the following units for velocity, length and time respectively:

$$v_0 = \left[\frac{2}{\beta^3}\frac{B D_T \nu_1 W_1}{\rho} Y_{0u}\exp\left\{-\frac{E}{RT_b}\right\}\right]^{1/2}, \quad L_0 = D_T/v_0, \quad t_0 = D_T/v_0^2. \tag{2.10}$$

Here T_b is the adiabatic flame temperature, and $\beta = E(T_b - T_u)/RT_b^2$ is the Zeldovich number; v_0 is the classical leading-order asymptotic result for the propagation velocity of a planar premixed flame propagating in a stoichiometric mixture. The dimensionless variables are defined by

$$t = \tilde{t}/t_0, \qquad r = \tilde{r}/L_0, \qquad z = \tilde{z}/L_0, \tag{2.11}$$

$$\theta = (T - T_u)/(T_b - T_u), \qquad y_i = Y_i/Y_{iu}. \tag{2.12}$$

According to the definition of the heat of reaction we then have

$$C_p(T_b - T_u)\left(\frac{\nu_0 W_0}{Y_{0u}} + \frac{\nu_1 W_1}{Y_{1u}}\right) = Q, \tag{2.13}$$

which determines the adiabatic flame temperature T_b. With the constant-density approximation, the heat release parameter $\alpha = (T_b - T_u)/T_b \ll 1$. Consequently, in non-dimensional form, the conservation equations (2.2) and (2.3) become

$$\frac{\partial\theta}{\partial t} + \lambda r\frac{\partial\theta}{\partial r} - 2\lambda z\frac{\partial\theta}{\partial z} = \frac{1}{r}\frac{\partial}{\partial r}\left(r\frac{\partial\theta}{\partial r}\right) + \frac{\partial^2\theta}{\partial z^2} + \beta^3 y_0 y_1 \exp\{-\beta(1-\theta)\}, \tag{2.14}$$

$$\frac{\partial y_i}{\partial t} + \lambda r\frac{\partial y_i}{\partial r} - 2\lambda z\frac{\partial y_i}{\partial z} = \frac{1}{Le}\left[\frac{1}{r}\frac{\partial}{\partial r}\left(r\frac{\partial y_i}{\partial r}\right) + \frac{\partial^2 y_i}{\partial z^2}\right] - \tfrac{1}{2}\beta^3 y_0 y_1 \exp\{-\beta(1-\theta)\}, \tag{2.15}$$

where $Le = D_T/D$ is the Lewis number, and $\lambda = aD_T/v_0^2$ is the dimensionless strain rate parameter.

In this paper we study only the unity Lewis number case. Hence, the fuel mixture fraction

$$Z = \frac{1 + y_0 - y_1}{2} \tag{2.16}$$

satisfies

$$\frac{\partial Z}{\partial t} + \lambda r\frac{\partial Z}{\partial r} - 2\lambda z\frac{\partial Z}{\partial z} = \frac{1}{r}\frac{\partial}{\partial r}\left(r\frac{\partial Z}{\partial r}\right) + \frac{\partial^2 Z}{\partial z^2}, \tag{2.17}$$

which admits a steady solution

$$Z = \tfrac{1}{2}[1 + \operatorname{erf}(\sqrt{\lambda}\, z)]. \tag{2.18}$$

Since Lewis numbers are unity, y_0 and y_1 may be expressed as functions of Z and θ using the Shvab–Zeldovich reduction, so that (2.14) becomes

$$\frac{\partial\theta}{\partial t} + \lambda r\frac{\partial\theta}{\partial r} - 2\lambda z\frac{\partial\theta}{\partial z} = \frac{1}{r}\frac{\partial}{\partial r}\left(r\frac{\partial\theta}{\partial r}\right) + \frac{\partial^2\theta}{\partial z^2} + \beta^3\left(Z - \tfrac{1}{2}\theta\right)\left(1 - Z - \tfrac{1}{2}\theta\right)\exp\{-\beta(1-\theta)\}. \tag{2.19}$$

The boundary conditions (2.4) and (2.5) now take the dimensionless form

$$\left.\frac{\partial\theta}{\partial r}\right|_{r=0,\infty} = 0, \qquad \theta(z \to \pm\infty) = 0. \tag{2.20}$$

Equations (2.18) and (2.19) together with the boundary conditions (2.20) and appropriate initial conditions define the problem that we will be solving numerically in this paper. The dimensionless parameters of interest are the strain rate λ and the Zeldovich number β. The initial conditions are discussed in the next section.

3. Method of solution

Equation (2.19) will be solved numerically using a finite difference method. Without loss of generality, we will choose a fixed Zeldovich number $\beta = 16$ in all of the following simulations. Clearly, the temperature field θ is symmetrical with respect to the stagnation plane $z = 0$, so it is sufficient to choose a two-dimensional computational domain $[0, r_{max}] \times [0, z_{max}]$ with an adiabatic boundary condition $\partial\theta/\partial z(z = 0) = 0$. The upper boundary z_{max} is chosen to be large enough such that $Z(z_{max}) \approx 1$. The boundary condition for temperature at $z = z_{max}$ may then be approximated by $\theta(z_{max}) = 0$. The choice of z_{max} depends on the strain rate λ. The radial boundary has been chosen as $r_{max} = 20$ in this paper, with Neumann boundary condition $\partial\theta/\partial r(r = r_{max}) = 0$.

The computational domain is discretized by uniformly spaced grid points in both the radial and transverse directions. Spatial derivatives are discretized by the sixth-order compact finite difference scheme (Lele 1992). For time integration, a simple forward Euler time stepping is used. Though less robust and accurate than, say, the fourth-order Runge–Kutta method, the ease of implementation and speed of calculations dictated our choice. In a similar calculation of colliding planar premixed flames (Lu & Ghosal 2003), we have compared these two time integration methods; the discrepancy turned out to be negligibly small. The initial conditions are specified in the following manner. For the flame hole problem, suppose that a steady diffusion-flame sheet has been established on the stagnation plane, we then artificially create a circular extinction hole on the flame sheet with centre at the stagnation point and initial hole radius r_i; similarly for the flame disk problem, except that the ignited and extinguished regions are interchanged. In terms of symbols, the initial conditions are

$$\theta(z, r) = \begin{cases} 0, & 0 \leqslant r \leqslant r_i \\ \theta_s(z; \lambda), & r_i < r \leqslant r_{max} \end{cases} \quad \text{for flame holes,} \tag{3.1a}$$

$$\theta(z, r) = \begin{cases} \theta_s(z; \lambda), & 0 \leqslant r \leqslant r_i \\ 0, & r_i < r \leqslant r_{max} \end{cases} \quad \text{for flame disks.} \tag{3.1b}$$

The calculation of $\theta_s(z; \lambda)$, which represents the temperature profile of a steady diffusion flame for strain rate λ, is addressed in § 4.

4. The steady diffusion-flame sheet

For a steady axisymmetric counterflow diffusion flame, (2.19) reduces to the following ordinary differential equation with respect to z:

$$\frac{\mathrm{d}^2\theta}{\mathrm{d}z^2} + 2\lambda z \frac{\mathrm{d}\theta}{\mathrm{d}z} + \beta^3 \left(Z - \tfrac{1}{2}\theta\right)\left(1 - Z - \tfrac{1}{2}\theta\right) \exp\{-\beta(1 - \theta)\} = 0 \tag{4.1}$$

with boundary conditions on the computational domain $[0, z_{max}]$

$$\left.\frac{\mathrm{d}\theta}{\mathrm{d}z}\right|_{z=0} = 0, \qquad \theta(z = z_{max}) = 0. \tag{4.2}$$

This is a nonlinear two-point boundary value problem with λ as a control parameter. A shooting method has been used to obtain its solution. Equation (4.1) is first transformed to two coupled first-order ordinary differential equations with θ and $\mathrm{d}\theta/\mathrm{d}z$ as the two dependent variables. Then, for each λ, an appropriate left-hand boundary value of temperature, $\theta(z = 0)$, which is also the maximum temperature

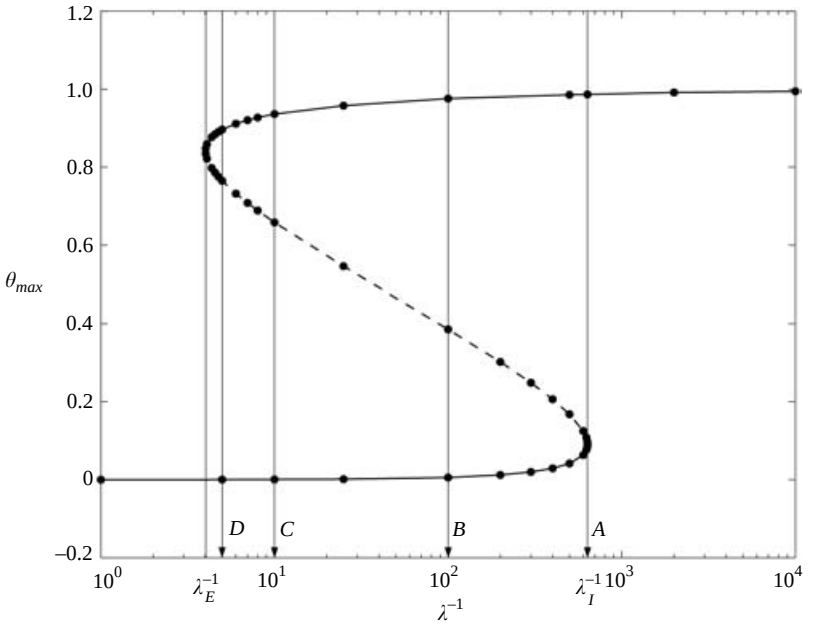

FIGURE 2. The S-shaped response curve for an axisymmetric counterflow diffusion flame: ●, calculation data points; ——, the extinguished and ignited branches; – – – – –, the unstable intermediate branch.

Case	λ	θ_{max} (ignited branch)	$v_{f\infty}$
A	0.00158	0.9865	0.9464
B	0.01	0.9758	0.7313
C	0.1	0.9360	0.1309
D	0.2	0.8962	–0.7186

TABLE 1. Four representative cases with strain rates within the extinction and ignition limits.

in the domain, is sought such that after integration of the system, the right-hand boundary gives $\theta(z_{max}) = 0$. The integration technique is a fifth-order Runge–Kutta method with adaptive stepsize control. The maximum temperature θ_{max} plotted against the inverse of the strain rate, λ^{-1}, is shown in figure 2. As can be seen, it is the well-known S-shaped response curve. Two critical strain rates, $\lambda_I \approx 0.00158$ and $\lambda_E \approx 0.239$, which correspond to ignition and extinction strain rates respectively, divide the continuous S-curve into three branches – a lower extinguished branch, an upper ignited branch, and an intermediate unstable branch.

The S-curve is the reference point of our investigation of the flame hole and flame disk problem. As noted by Buckmaster & Jackson (2000), the edge of the flame hole (disk) serves as a transition structure between the extinguished and ignited branches of the S-curve, and it is the ability of the edge flame to propagate that determines the dynamical properties of the flame hole (disk). In the following simulations, we will choose four representative cases *A*–*D* within the interval between λ_I and λ_E, as listed in table 1 and marked in figure 2. Also shown in table 1 is $v_{f\infty}$, the edge-flame propagation velocity when the hole (disk) radius r_f approaches infinity, that

is, the propagation velocity of a straight edge flame. It is seen that $v_{f\infty}$ increases with decreasing of the strain rate λ, and there exists a critical strain rate λ_c, which is somewhere between 0.1 and 0.2 (between C and D in figure 2), at which $v_{f\infty}$ vanishes. Thus, λ_c is the critical point between a deflagration front and a failure wave. It should be emphasized that this is applicable only for a straight edge flame. As will be seen later in § 5 and § 6, when the edge curvature effects are taken into account, both deflagration fronts and failure waves can exist for any strain rate within the interval $[\lambda_I, \lambda_E]$.

For each of cases A–D, we will need to calculate the steady temperature profile $\theta_s(z;\lambda)$ corresponding to the ignited branch. This is done by using a straightforward relaxation method; equation (4.1) is transformed to an unsteady equation by adding an unsteady term $\partial\theta/\partial t$ on the left-hand side, then an appropriate guessed temperature profile is chosen as the initial condition to iterate the unsteady equation until the steady solution, $\theta_s(z;\lambda)$, is obtained.

5. Circular holes on a diffusion-flame sheet

We consider the axisymmetric counterflow diffusion flame with strain rate λ, and suppose that on the flame sheet there is a circular extinction hole with centre at the origin and hole radius r_i. This corresponds to the initial condition defined by equation (3.1*a*).

After a short transient time, the discontinuous temperature profile will evolve into a smooth circular edge-flame front, which, depending on the strain rate λ and the size of the hole, may propagate inward as an ignition front or outward as an extinction front. In order to investigate the dynamical properties of the flame hole, one needs to define the instantaneous location of the hole edge. Generally this definition is not unique due to the finite size of the reaction zone. In their simulations, Buckmaster & Jackson (2000) tracked the temperature contour and the edge location was identified with the point where the temperature is 80% of the Burke–Schumann value. In this paper, the instantaneous edge location $r_f(t)$ is identified with the radial coordinate of the point P at which the reaction rate ω reaches its maximum. Clearly, P is always located on the stagnation plane $z = 0$.

Figure 3 shows the instantaneous radial reaction rate profiles of flame holes on the stagnation plane $z = 0$ for four different strain rates, that is, cases A–D (cf. table 1 and figure 2). The existence of a well-defined reaction rate peak is apparent – though less easily discernible for high strain rates (such as case D). Nevertheless the value of r corresponding to the maximum of the reaction rate can still be uniquely identified.

5.1. *Critical hole radius*

The dynamical behaviour of the flame hole is determined by two parameters, the strain rate λ and the instantaneous hole radius r_f. The balance between heat generation and diffusional heat losses is now complicated by the role of the hole curvature effects and the counterflow velocity field. If the favourable effects dominate, the hole edge-flame front will propagate inward to close the hole; otherwise the hole will expand outward to enlarge the extinction area. For a fixed strain rate λ, there exists a critical hole radius r_c at which a balance is reached, characterized by a stationary hole edge. The critical radius is an unstable bifurcation point that separates the shrinking and expanding hole regimes. Figure 4 shows the critical hole radius r_c for the entire range of strain rates within the interval $[\lambda_I, \lambda_E]$. The method of determination of the critical radius is described in § 5.3. Here, we only point out that r_c increases

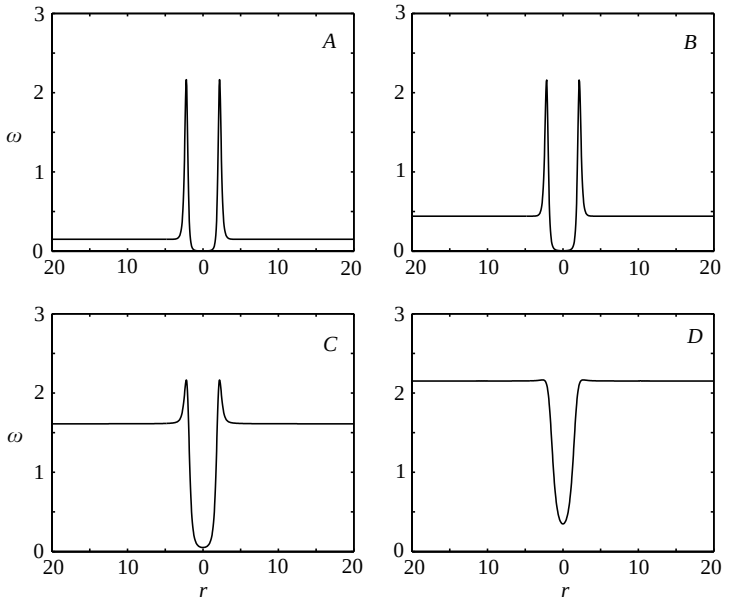

FIGURE 3. Instantaneous radial reaction rate profiles of flame holes on the stagnation plane $z = 0$ for cases A–D for the same value of the hole radius.

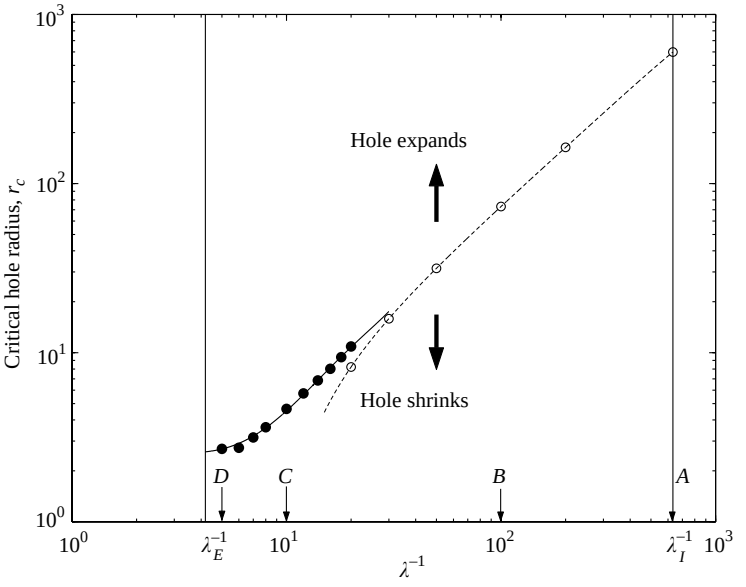

FIGURE 4. The flame hole critical radius as a function of strain rate: ●, from numerical simulation data; ——, fourth-order polynomial fit; ○, $r_c = v_{f\infty}(\lambda)/\lambda$; – – – – –, spline fit.

monotonically with decreasing of the strain rate, as seen in figure 4, and postpone a detailed discussion of this issue to § 5.3.

5.2. *Flame topology*

The temporal evolution of a collapsing flame hole in its final stage, as represented by the cross-sectional view of the isocontours of the reaction rate, is shown in figure 5.

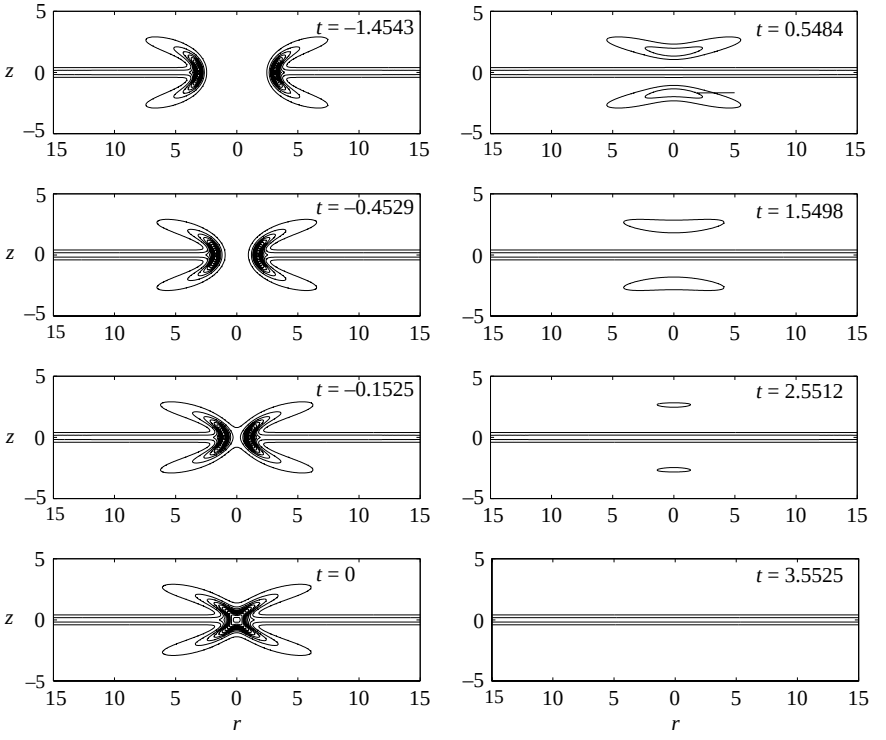

FIGURE 5. Temporal evolution of isocontours of reaction rate of a collapsing flame hole for case *B* (cf. figure 2) – cross-sectional view.

The counterflow strain rate is $\lambda = 0.01$ corresponding to case *B* in table 1 and figure 2. It can be clearly seen that the hole edge exhibits a triple flame structure in cross-section, with its convex side pointing to the centre of the hole. As a result, the hole edge is characterized by a saddle-like topological structure, associated with two orthogonal curvatures: the curvature of the partially premixed front and the inverse of the hole radius.

As can be seen from figure 5, the collapse of a flame hole can be divided into two stages. The first is the collapsing stage in which the hole shrinks until the hole edge converges to a point at the centre. We take this moment as the point of reference of time, $t = 0$. The time preceding this moment (the collapsing stage) is taken as negative. Next comes the post-collapse stage. The residual rich and lean premixed edge flame fronts separate themselves immediately from the main diffusion flame to form two flame isolas on two sides of the diffusion flame sheet. They then gradually die out and a steady diffusion flame is established.

However, when the strain rate is relatively large, the collapsing flame hole may exhibit qualitatively different features. Figure 6 shows the temporal evolution of a flame hole for case *C* ($\lambda = 0.1$) when the flame is highly strained and close to the extinction limit (cf. figure 2). As can be seen, unlike the previous case, the hole edge does not have an apparent triple flame structure; instead, it degenerates into a simple blunt edge. Accordingly, there is no clear post-collapse stage. The blunt hole edge shrinks to the centre and then gradually flattens out.

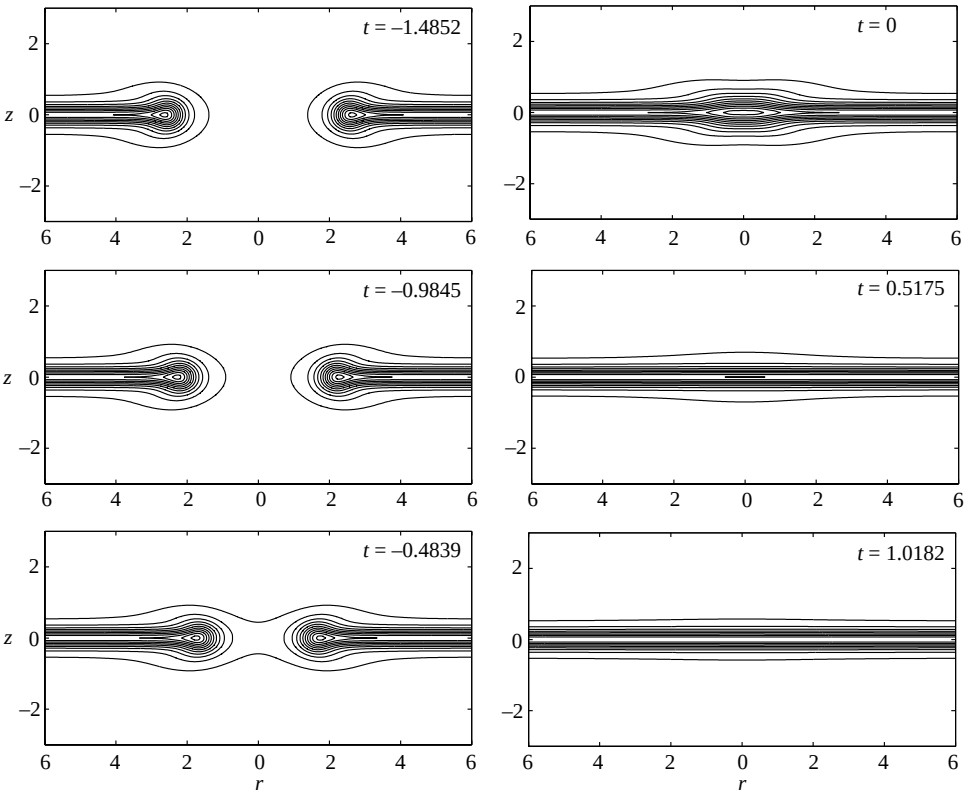

FIGURE 6. Temporal evolution of isocontours of reaction rate of a collapsing flame hole for case C (cf. figure 2) – cross-sectional view.

5.3. *Dynamics of flame holes*

How does the hole edge travelling speed, $-\mathrm{d}r_f/\mathrm{d}t = f(r_f, \lambda)$, depend on the strain rate λ and the instantaneous hole radius r_f? We attempt to determine the function $f(r_f, \lambda)$ using our numerical simulations.

Recently, Pantano & Pullin (2003) employed Buckmaster's one-dimensional edge-flame model (Buckmaster 1996) to obtain an asymptotic solution for the evolution of a shrinking flame hole edge in the limit of large activation energy. They concluded that in the final stages of collapse, the flame hole shrinks according to a 1/2-power of time remaining to collapse. That is, in our notation,

$$r_f(t) = \sqrt{-6.31982\, t}. \tag{5.1}$$

The trajectories of a collapsing flame hole edge for cases A–D are shown in figure 7. Equation (5.1) is plotted as the dashed line. As can be seen, the agreement between the theory and our numerical results is excellent for small (case A) and moderate (case B) strain rates (the hole edge possesses the triple flame structure), while for high strain rates (cases C,D; the hole edge possesses simple blunt edge structure) the agreement is less satisfactory.

Figure 8 shows the phase diagram of flame holes for cases A–D, represented by the edge travelling speed, $-\dot{r}_f(t)$, against the instantaneous hole radius $r_f(t)$. Following Buckmaster & Jackson (2000), different initial hole radii r_i for each strain rate have been tested and it turns out that for a given strain rate, all of these phase curves

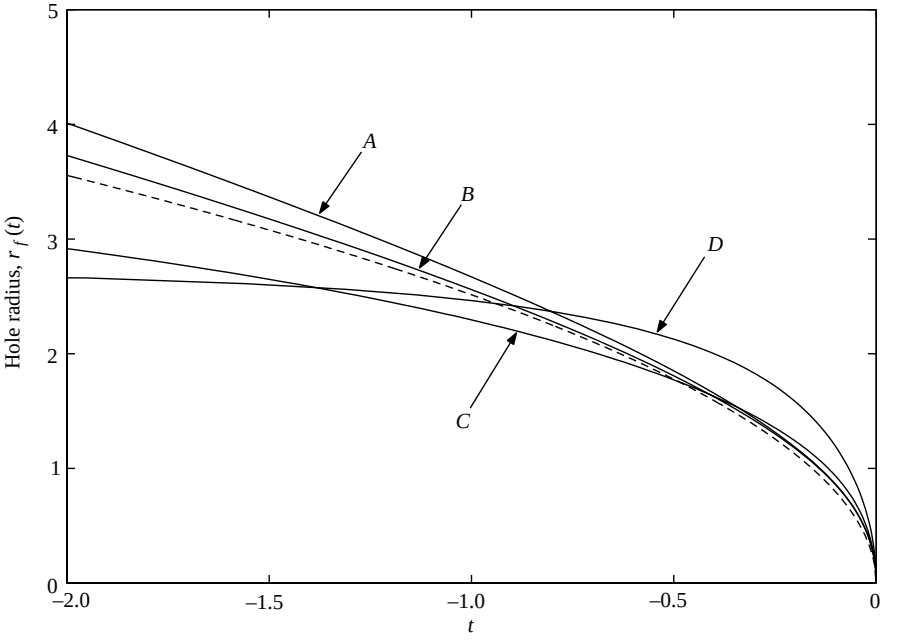

FIGURE 7. Trajectory of the shrinking flame hole radius: ——, numerical calculations; – – – – –, $r_f = (-6.31982\,t)^{1/2}$ (Pantano & Pullin 2003).

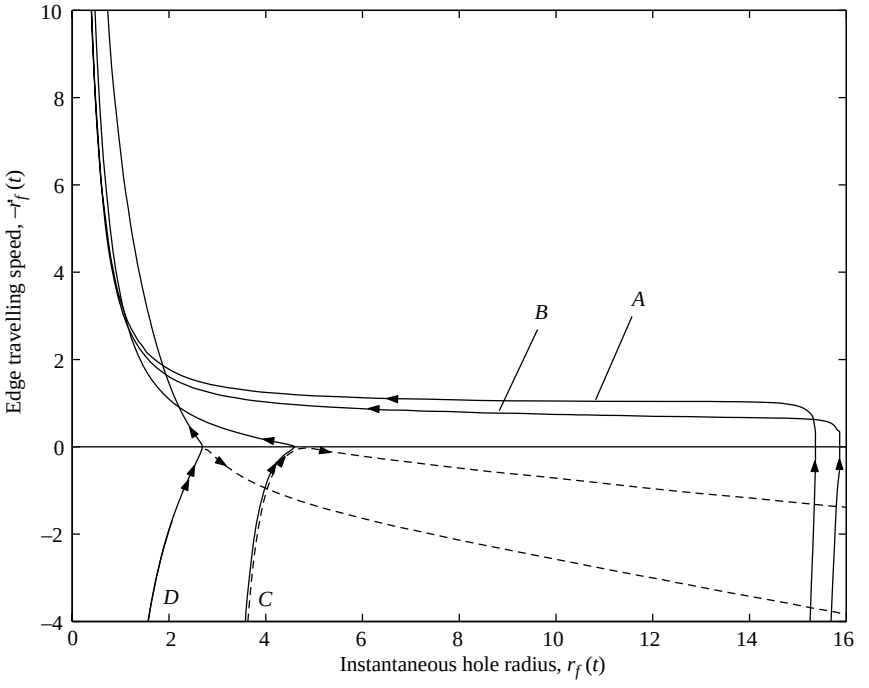

FIGURE 8. Phase diagram of flame holes: ——, shrinking regime; – – – – –, expanding regime. Arrows indicate the hole edge travelling direction.

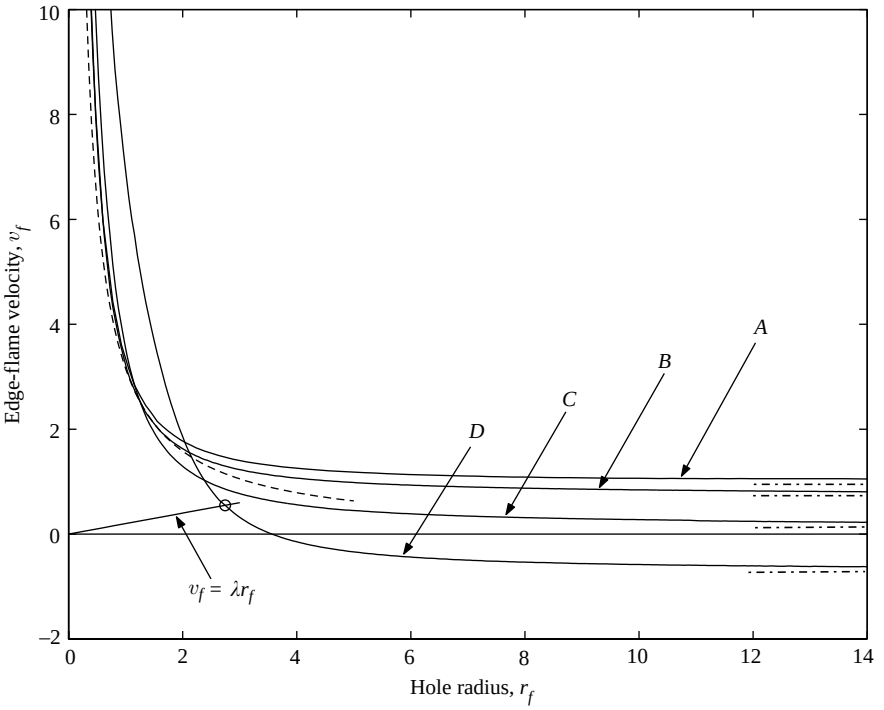

FIGURE 9. The hole edge-flame velocity as a function of hole radius: ——, numerical results; —·—, straight edge-flame velocity ($r_f \to \infty$); – – – –, $v_f = 3.15991/r_f$ (Pantano & Pullin 2003). The circle symbol marks the location of the critical hole radius for case D.

collapse on to a unique curve $f(r_f, \lambda)$ after a short transient time. For each of the cases, C and D, a pair of values for the initial hole radius was carefully chosen such that after a short transient, one corresponds to a hole that is slightly smaller than the critical hole radius r_c and the other corresponds to a hole only slightly larger than r_c. The two phase curves evolve to two branches that close and expand the hole, respectively. As can be clearly seen from figure 8, the collapsing and expanding branches connect at the critical hole radius and constitute a smooth phase curve, $f(r_f, \lambda)$. To determine the location of the critical hole radius, a data fitting of the two branches in the vicinity of r_c has been employed and the intersection point of the connected smooth phase curve and the $\dot{r}_f = 0$ line locates the critical hole radius.

Let us define an edge-flame propagation velocity v_f as the edge travelling velocity relative to the gas. Thus, for the present flame hole problem, $v_f = -\dot{r}_f + \lambda r_f$. The edge-flame propagation velocities against the hole radius r_f for cases A–D are shown in figure 9. The corresponding propagation velocities of straight edge flames, $v_{f\infty}$ (see table 1), are marked in figure 9 as dash-dot lines. Pantano & Pullin's (2003) prediction of edge flame velocity, a direct differentiation of (5.1), $v_f = 3.15991/r_f$, is also plotted as the dashed line. It is evident that when r_f is sufficiently large, the curvature effects of the flame hole are weak and the edge-flame propagation velocity approaches the value of the corresponding straight edge flame, $v_{f\infty}$. However, with decrease of the hole radius, the curvature of the hole edge will reduce the heat losses and thus gradually enhance the edge-flame velocity. When r_f becomes of the order of the edge flame thermal thickness ($O(1)$ in present formulation), all flame elements on the hole edge interact by overlapping of their preheat zones. This flame

interaction leads to a substantial increase of the edge flame velocity. Qualitatively, this acceleration mechanism is similar to that of the head-on collision of two planar premixed flames (Chen & Sohrab 1995; Lu & Ghosal 2003), except that the focusing effects of a flame hole enhance the acceleration further.

Now let us go back to the discussion of the critical hole radius. According to the definition of the critical hole radius, we have $v_f(r_c) = \lambda r_c$. Hence, the intersection point of the straight line $v_f = \lambda r_f$ and the corresponding $v_f(r_f)$ curve determines the location of the critical hole radius r_c, as marked by the circle symbol in figure 9. When the strain rate is very small, r_c is large and $v_f \approx v_{f\infty}(\lambda)$, so that $r_c \approx v_{f\infty}(\lambda)/\lambda$, which is plotted in figure 4 as open circle symbols. It can be seen that with the increase of the strain rate, the critical hole radius obtained in this way gradually deviates from the directly calculated results (marked by bullet symbols in figure 4) because of the acceleration of the edge-flame velocity. The limiting value of r_c when the strain rate approaches the extinction limit λ_E is of interest. This is determined for a number of values of λ in the range $0.05 \leqslant \lambda < \lambda_E$ in the manner discussed earlier and a fourth-order polynomial fit is used in figure 4 to obtain r_c close to the extinction limit. It is seen from figure 4 that the critical hole radius at the extinction limit, λ_E, is a finite value $r_c \approx 2.7$. This indicates that regardless of the strain rate, as long as a diffusion flame exists, it cannot be destroyed by making an infinitesimal extinction hole in it. This is in agreement with the inference of Buckmaster & Jackson (2000) in the absence of a straining velocity field.

6. Circular flame disks on a stoichiometric plane

Compared with the flame hole problem, the effects of disk curvature and counterflow velocity field are reversed for a flame disk. As before, we begin with a study of the topological structure of the flame disks.

6.1. *Flame topology*

Figure 10 shows the evolution of an expanding flame disk for case *B*. After a short transient time, the initial small flame disk evolves into a flame ball that expands like a spherical expanding front. Because of the effects of the mixture fraction gradient in the lateral direction, the expansion velocity of the flame ball is not isotropic – it is fastest on the stoichiometric plane and slowest along the symmetry axis. As a result, the flame ball gradually evolves into an ellipsoid which is composed of partially premixed flame fronts. The lean and rich burning flame elements leave behind excess oxidizer and fuel respectively to cause an accumulation of heated fuel and oxidizer inside the ellipsoid. These residual gases come together at the stoichiometric plane and establish a diffusion flame. With further expansion of the flame surface, the partially premixed flame fronts propagating into the fuel and oxidizer become weaker because of lack of fuel and oxygen, and soon the ellipsoid evolves into an annular triple flame propagating outward and trapping an expanding diffusion flame inside. Qualitatively, this process is very similar to ignition from a point source in a non-premixed turbulent two-dimensional flow described earlier by Domingo & Varvisch (1996).

For large strain rates, as in the previously discussed flame hole problem, the triple flame structure is replaced by a blunt edge (cf. figure 6).

6.2. *Dynamics of flame disks*

The phase diagram of flame disks for cases *A*–*D* is given in figure 11. It is evident that corresponding to each strain rate, there exists a critical disk radius r_c that separates

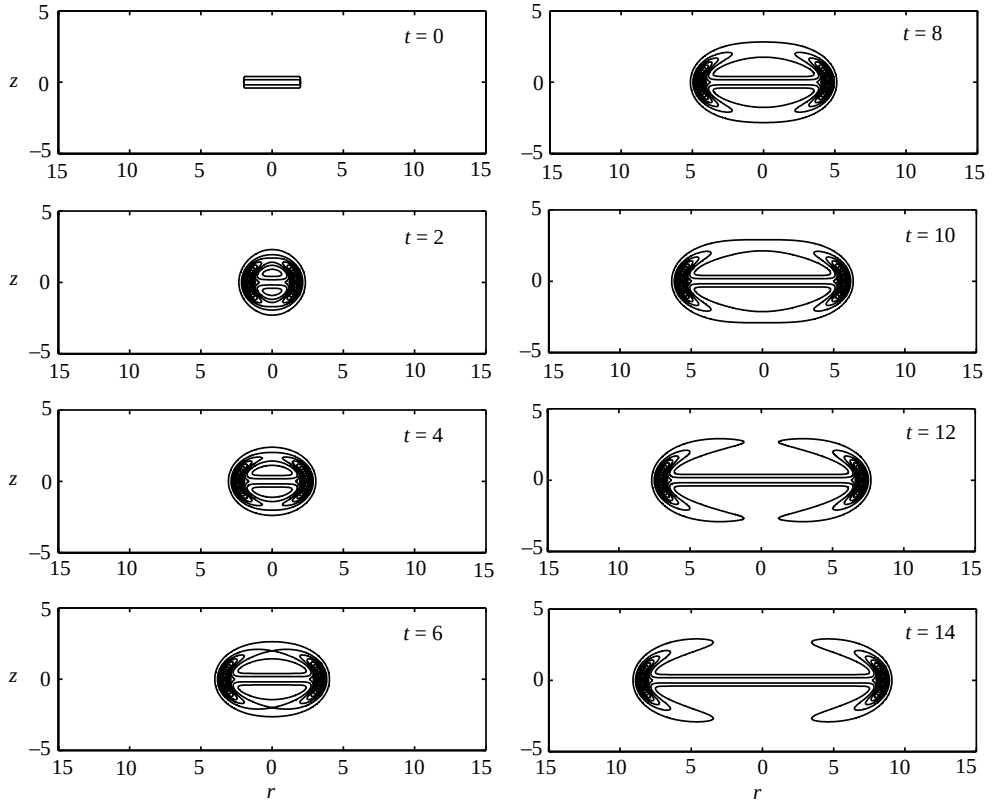

FIGURE 10. Temporal evolution of isocontours of reaction rate of an expanding flame disk for case B (cf. figure 2) – cross-sectional view.

the expanding and shrinking branches of the phase curve. The critical disk radius against the inverse of the strain rate, determined by using the same method as before, is shown in figure 12. It is seen that r_c decreases with decrease of the strain rate and reaches its minimum $r_{c_{min}} = 0.83$ at the ignition limit λ_I. This gives the minimum flame disk radius below which a counterflow mixing layer cannot be ignited. As noted in § 6.1, for relatively small strain rates, the expansion of a small flame disk in a mixing layer corresponds to the after-transient stage of ignition by a point energy source. From a general point of view, the small flame disk may also be thought of as a planar source. It is known that for these kinds of ignition energy sources, point or planar, there exists a critical energy value such that the initial flame kernel could evolve to a self-propagating flame only if the energy released by the source is greater than this critical value (see Vázquez-Espí & Liñán 2002). In this sense, the critical disk radius r_c may be inherently related to the critical energy of the ignition source.

The edge-flame velocity for a flame disk now takes the form $v_f = \dot{r}_f - \lambda r_f$. The edge-flame velocities plotted against the disk radius r_f for cases A–D are shown in figure 13. The corresponding straight edge-flame velocities, $v_{f\infty}$, are marked by dash-dot lines. It is seen that for different strain rates, the general tendency is: v_f gradually decreases from $v_{f\infty}$ at infinity with decrease of the disk radius, and when r_f is of the same order as the edge-flame thickness ($O(1)$), v_f decreases sharply until eventual annihilation of the flame disk. Compared with the flame hole problem, there are no upstream flame interactions in this case. Therefore, it is expected that the

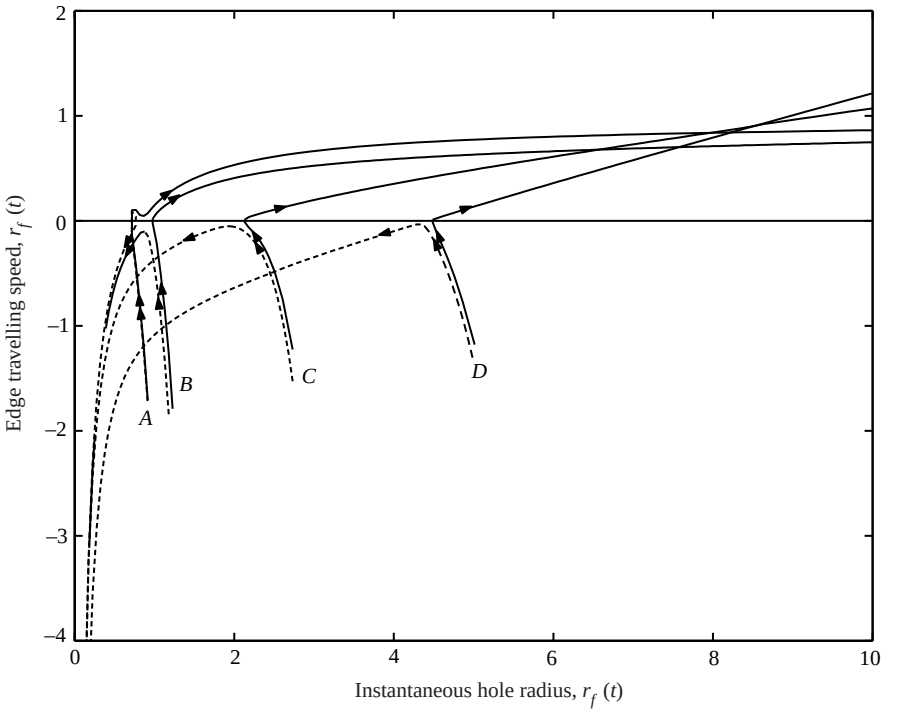

FIGURE 11. Phase diagram of flame disks: ——, expanding regime; – – – –, shrinking regime. Arrows indicate the disk edge travelling direction.

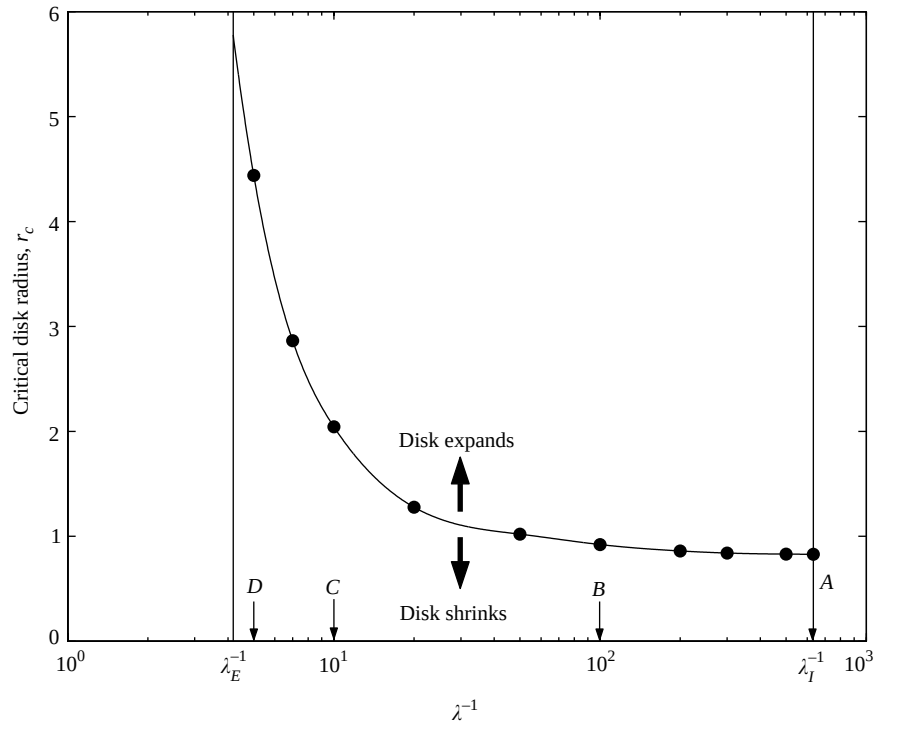

FIGURE 12. The flame-disk critical radius as a function of strain rate: ●, from numerical simulation data; ——, spline fit.

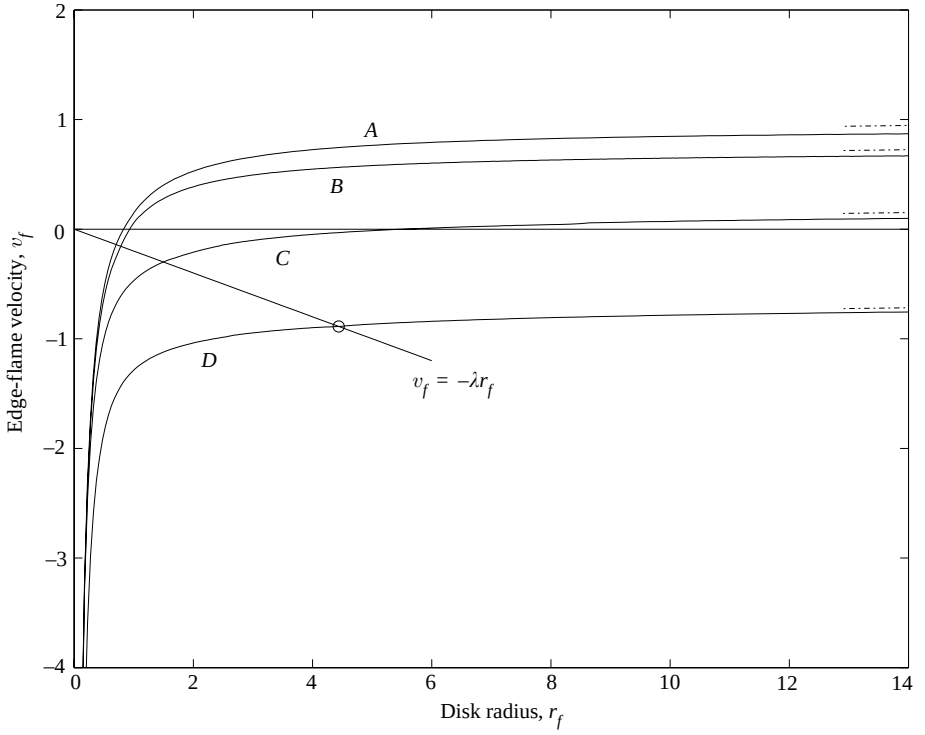

FIGURE 13. The disk edge-flame velocity as a function of disk radius: —·—, straight edge-flame velocity ($r_f \to \infty$). The circle symbol marks the location of the critical disk radius for case *D*.

increasing curvature effects will play a major role in the acceleration (in the negative direction) of the edge-flame velocity, caused by the increasing heat loss rate.

7. Conclusion

A numerical investigation of flame holes and flame disks in a laminar axisymmetric counterflow configuration is presented. The time-varying topological structure of the flame edge is described and the dynamical behaviour of edge flames in the shrinking and expanding processes of flame holes and flame disks is investigated.

It was found that for both flame holes and flame disks, there exists a critical radius r_c, which is an unstable bifurcation point and separates the shrinking and expanding flame hole (disk) regimes. For a flame hole (disk), the critical radius increases (decreases) monotonically with decreasing of the strain rate within the interval formed by the extinction and ignition strain rates, and reaches a finite minimum at the extinction (ignition) limit. This implies that a mixing layer cannot be ignited by an infinitesimal energy source, nor can a flame sheet, once established, be quenched by poking an infinitesimal extinction hole on it.

In the phase diagram, it was found that for a given strain rate, the phase curves that begin from different initial radii, after a short transient, all collapse to two unique enveloping branches of a smooth continuous phase curve. This indicates that an edge travelling speed defined as a function of hole (disk) radius, strain rate (or equivalently, Damköhler number) as well as other relevant combustion parameters

(such as the Zeldovich number etc.), is a meaningful concept not only for shrinking flame holes and shrinking flame disks (as noted by Buckmaster & Jackson 2000), but also for expanding flame holes and expanding flame disks. Corresponding to the edge travelling speed, the edge-flame velocity v_f is also a smooth continuous function of radius and strain rate in the entire range of hole (disk) radius $0 < r_f < \infty$. Edge-flame velocity v_f approaches the corresponding propagation velocity of a straight edge flame when r_f goes to infinity and tends to very large positive and negative values for flame holes and flame disks, respectively, when r_f approaches zero. For flame holes, it is found that the edge-flame velocity is essentially proportional to the inverse of the hole radius in the final collapsing stage, except when the strain rate is within a short interval that is close to the extinction limit. The flame interactions caused by overlapping of pre-heat zones are mainly responsible for this acceleration mechanism, and it is further enhanced by the focusing effects of the continuously increasing hole curvature. For flame disks, the acceleration (in the negative direction) of the edge-flame velocity is mainly caused by the increasing heat loss rate.

The effect of heat release on two-dimensional isolated triple flames was numerically investigated by Ruetsch *et al.* (1995), which was followed later by an analytical study by Ghosal & Vervisch (2000) using activation energy asymptotics. The simulation results of Ruetsch *et al.* (1995) showed that thermal density variations affect the flow structure around the flame, with the result that the propagation velocity of the triple flame is increased. In fact, the triple flame can actually propagate faster than the corresponding stoichiometric planar flame, a somewhat unexpected result. For the current flame hole and flame disk problem, when the hole (disk) radius is large enough, the curvature in the stoichiometric plane is not significant and the results for isolated triple flames with heat release mentioned previously should be recovered. The more interesting situation arises as the hole (disk) radius shrinks. In this case one expects a radial outflow of gas due to thermal expansion and deviation of the streamlines in the vicinity of the edge would also result in modification of the mixture fraction ahead of the edge flame. This should alter the dynamics of collapse in an essential way. The simulations presented in this paper do not take this effect into account, and are therefore qualitatively applicable to situations where density variations are negligible; for example if the fuel and oxidizer are greatly diluted with an inert species.

This work was supported by the National Science Foundation under grant No. CTS-0121051. We also thank Luc Vervisch for providing the original code which we modified to perform the numerical simulations.

REFERENCES

Buckmaster, J. 1996 Edge-flames and their stability. *Combust. Sci. Technol.* **115**, 41–68.

Buckmaster, J. 1997 Edge-flames. *J. Engng Maths* **31**, 269–284.

Buckmaster, J. 2002 Edge-flames. *Prog. Energ. Combust. Sci.* **28**, 435–475.

Buckmaster, J. & Jackson, T. L. 2000 Holes in flames, flame isolas, and flame edges. In *Proc. 28th Symp. (Intl) Combust.*, pp. 1957–1964. The Combustion Institute.

Buckmaster, J. & Matalon, M. 1988 Anomalous Lewis number effects in tribrachial flames. In *Proc. 22nd Symp. (Intl) Combust.*, pp. 1527–1535. The Combustion Institute.

Cha, C. M., Kosaly, G. & Pitsch, H. 2001 Modeling extinction and reignition in turbulent nonpremixed combustion using a doubly-conditional moment closure approach. *Phys. Fluids* **13**, 3824–3834.

Cha, C. M. & Pitsch, H. 2002 Higher-order conditional moment closure modelling of local extinction and reignition in turbulent combustion. *Combust. Theory Modelling* **6**, 425–437.

Chen, C. L. & Sohrab, S. H. 1995 Upstream interactions between planar symmetric laminar methane premixed flames. *Combust. Flame* **101**, 360–370.

Daou, J. & Liñán, A. 1998 The role of unequal diffusivities in ignition and extinction fronts in strained mixing layers. *Combust. Theory Modelling* **2**, 449–477.

Dold, J. W. 1989 Flame propagation in a nonuniform mixture: analysis of a slowly varying triple flame. *Combust. Flame* **76**, 71–88.

Domingo, P. & Vervisch, L. 1996 Triple flames and partially premixed combustion in auto-ignition of non-premixed mixtures. In Proc. *26th Symp. (Intl) Combust*., pp. 233–240. The Combustion Institute.

Echekki, T. & Chen, J. H. 1998 Structure and propagation of methanol-air triple flames. *Combust. Flame* **114**, 231–245.

Favier, V. & Vervisch, L. 1998 Investigating the effects of edge-flames in liftoff in non-premixed turbulent combustion. In *Proc. 27th Symp. (Intl) Combust*., pp. 1239–1245. The Combustion Institute.

Ghosal, S. & Vervisch, L. 2000 Theoretical and numerical study of a symmetrical triple flame using the parabolic flame path approximation. *J. Fluid Mech.* **415**, 227–260.

Hartley, L. J. & Dold, J. W. 1991 Flame propagation in a nonuniform mixture: analysis of a propagating triple-flame. *Combust. Sci. Technol.* **80**, 23–46.

Im, H. G. & Chen, J. H. 1999 Structure and propagation of triple flames in partially premixed hydrogen-air mixtures. *Combust. Flame* **119**, 436–454.

Kim, S. H., Huh, K. Y. & Bilger, R. W. 2002 Second-order conditional moment closure modeling of local extinction and reignition in turbulent non-premixed hydrocarbon flames. In *Proc. 29th Symp. (Intl) Combust*., pp. 2131–2137. The Combustion Institute.

Kioni, P. N., Rogg, B., Bray, K. N. C. & Liñán, A. 1993 Flame spread in laminar mixing layers: the triple flame. *Combust. Flame* **95**, 276–290.

Ko, Y. S. & Chung, S. H. 1999 Propagation of unsteady tribrachial flames in laminar non-premixed jets. *Combust. Flame* **118**, 151–163.

Lee, B. J. & Chung, S. H. 1997 Stabilization of lifted tribrachial flames in a laminar non-premixed jet. *Combust. Flame* **109**, 163–172.

Lele, S. K. 1992 Compact finite difference schemes with spectral-like resolution. *J. Comput. Phys.* **103**, 16–42.

Lu, Z. & Ghosal, S. 2003 A similarity solution describing the collision of two planar premixed flames. *Combust. Theory Modelling* **7**, 645–652.

Mauss, F., Keller, D. & Peters, N. 1990 A Lagrangian simulation of flamelet extinction and re-ignition in turbulent jet diffusion flames. In *Proc. 23rd Symp. (Intl) Combust*., pp. 693–698. The Combustion Institute.

Nayagam, V., Balasubramaniam, R. & Ronney, P. D. 1999 Diffusion flame-holes. *Combust. Theory Modelling* **3**, 727–742.

Nayagam, V. & Williams, F. A. 2001 Diffusion-flame dynamics in von Karman boundary layers. *Combust. Flame* **125**, 974–981.

Pantano, C. & Pullin, D. I. 2003 On the dynamics of the collapse of a diffusion-flame hole. *J. Fluid Mech.* **480**, 311–332.

Papas, P. & Tomboulides, A. G. 2000 Observations of annular-shaped edge flames in a counterflow. *Combust. Sci. Technol. Commun.* **1**, 13–16.

Peters, N. 1983 Local quenching due to flame stretch and non-premixed turbulent combustion. *Combust. Sci. Technol.* **30**, 1–17.

Phillips, H. 1965 Flame in a buoyant methane layer. In *Proc. 10th Symp. (Intl) Combust*., pp. 1277–1283. The Combustion Institute.

Pitsch, H., Cha, C. M. & Fedotov, S. 2003 Flamelet modelling of non-premixed turbulent combustion with local extinction and re-ignition. *Combust. Theory Modelling* **7**, 317–332.

Pitsch, H. & Fedotov, S. 2001 Investigation of scalar dissipation rate fluctuations in non-premixed turbulent combustion using a stochastic approach. *Combust. Theory Modelling* **5**, 41–57.

Plessing, T., Terhoeven, P., Peters, N. & Mansour, M. S. 1998 An experimental and numerical study of a laminar triple flame. *Combust. Flame* **115**, 335–353.

Ruetsch, G. R., Vervisch, L. & Liñán, A. 1995 Effects of heat release on triple flames. *Phys. Fluids* **7**, 1447–1454.

Santoro, V. S., Liñán, A. & Gomez, A. 2000 Propagation of edge flames in counterflow mixing layers: experiments and theory. In *Proc. 28th Symp. (Intl) Combust*., pp. 2039–2046. The Combustion Institute.

Schefer, R. W., Namazian, M., Filtopoulos, E. E. J. & Kelly, J. 1994 Temporal evolution of turbulence/chemistry interactions in lifted turbulent-jet flames. In *Proc. 25th Symp. (Intl) Combust*., pp. 1223–1231. The Combustion Institute.

Shay, M. L. & Ronney, P. D. 1998 Non-premixed edge flames in spatially varying straining flows. *Combust. Flame* **112**, 171–180.

Vázquez-Espí, C. & Liñán, A. 2002 Thermal-diffusive ignition and flame initiation by a local energy source. *Combust. Theory Modelling* **6**, 297–315.

Williams, F. A. 1975 Recent advances in theoretical descriptions of turbulent diffusion flames. In *Turbulent Mixing in Nonreactive and Reactive Flows* (ed. S. N. B. Murthy), pp. 189–208. Plenum.